Clinical Oral Implants Research

WILEY

CLINICAL ORAL IMPLANTS RESEARCH

ORIGINAL ARTICLE OPEN ACCESS

Dental Implant Osseointegration Following Mandibular Augmentation Using 3D Printed Hydroxyapatite Blocks. An Experimental In Vivo Study

Simon Systermans[1,2] | Christophe Ronsmans[2,3] | Grégory Nolens[4,5] | Joeri Meyns[6] | Yves Gilon[1] | Elisabeth Cobraiville[5,7]

[1]Department of Plastic and Maxillofacial Surgery, CHU Liège, Liège, Belgium | [2]Faculty of Medicine, University of Liège, Liège, Belgium | [3]Department of Plastic, Esthetic and Reconstructive Surgery, CHR Citadelle Liège, Liège, Belgium | [4]Faculty of Medicine, University of Namur, Namur, Belgium | [5]Cerhum SA, Liège, Belgium | [6]Department of Oral and Maxillofacial Surgery, ZOL Genk, Genk, Belgium | [7]GIGA-In Silico Medicine, Biomechanics Research Unit, University of Liège, Liège, Belgium

Correspondence: Elisabeth Cobraiville (elisabeth.cobraiville@doct.uliege.be; elisabeth.cobraiville@cerhum.com)

Received: 27 May 2025 | **Revised:** 19 September 2025 | **Accepted:** 24 September 2025

Funding: This work was supported by the DOVIMIS project, co-funded by Cerhum and the European Union's FEDER "Wallonie 2020.EU" program and the Walloon Region government under the program COOTECH MIX grant agreement No. 7931.

Keywords: 3D printing | alveolar ridge augmentation | dental implants | guided bone regeneration | oral surgery | osseointegration | scaffold | tissue engineering

ABSTRACT

Objective: To evaluate the use and osseointegration of dental implants in combination with 3D-printed hydroxyapatite (3DHA) blocks featuring gyroid porosity for large mandibular bone augmentation.

Methods: Mandibular lateral bone augmentation with gyroid-3DHA blocks was performed bilaterally on four female Göttingen minipigs. After 8 or 12 weeks of healing, a dental implant was placed into each 3DHA block. Following an additional 12-week healing period, the augmented sites (including 3DHA blocks and dental implants) were harvested for histological and histomorphometric analysis, assessing new bone formation, 3DHA integration, total bone gain, and bone-to-implant contact (BIC).

Results: Gyroid-3DHA blocks were easily fixated with screws. Dental implants were placed through the 3DHA blocks with a standard drilling procedure, and good primary stability was achieved. 3DHA blocks demonstrated good osseointegration with 39.17% of new bone and a significant bone gain of 4.73 mm on average. Dental implants showed comparable BIC within the 3DHA and into the native bone (42.79% vs. 34.17%). No significant difference was found between the healing periods.

Conclusion: This is the first study to evaluate a 3D-printed bone substitute in combination with a dental implant in an animal study. Gyroid-3DHA blocks and dental implants demonstrated good osseointegration, and the bone augmentation was significant, making it a promising material for large and complex alveolar ridge augmentations.

1 | Introduction

Dental implant placement to replace missing teeth is becoming more and more frequent. Alveolar ridge augmentations are therefore following the same trend. Conventional techniques for bone augmentation include autologous block grafting and guided bone regeneration (GBR) with bone particulates (either autogenous, derived from xenogeneic origin (bovine, equine, porcine), or particulates from alloplastic material). Autologous bone grafting is often successful but unpredictable, linked with donor site morbidity, and of limited availability. Additionally, the procedure requires advanced surgical skills. GBR with particulates and collagen membranes is efficient for horizontal augmentation and socket filling. However,

achieving good stability of the particulates in cases requiring substantial vertical augmentation or large augmentation remains challenging (Urban et al. 2023; Chao et al. 2017; Sanz-Sánchez et al. 2022).

Hydroxyapatite (HA) has been studied for decades for bone regeneration as it is the main constituent of the human bone (up to 70%). HA osseointegration properties have been demonstrated repeatedly and in various anatomical locations (Hou et al. 2022; Wang and Yeung 2017; Kattimani et al. 2016; Mohd et al. 2022; Habraken et al. 2016). Most of the time, HA bone substitutes are made of deproteinized bovine bone (Ferraz 2023) and provided in particulate shape, which does not adequately address the need for stability in vertical bone augmentation (Urban et al. 2023; Vaquette et al. 2022). Deproteinized bovine bone blocks fail to solve the issue also due to their high fragility impairing their fixation and their heterogeneity (Zecha et al. 2011; James et al. 2020). Therefore, synthetic HA blocks have been studied in the past to overcome these challenges, offering better stability. However, these HA blocks were usually associated with failure due to their lack of osseointegration, especially inside the block (Piecuch et al. 1990; Hupp and McKenna 1988; Alyahya and Swennen 2019), a consequence of inadequate porosity. Those blocks had an average pore size of 50 to 300 μm (Yoshikawa et al. 2008; White and Shors 1986; Cottrell and Wolford 1998) and pore interconnections of 40 μm (Yoshikawa et al. 2008). However, it has been demonstrated that macropores smaller than 100 μm can induce non-mineralized osteoid or fibrous tissue formation (Abbasi et al. 2020). It is recommended to have macropores of at least 400 μm to not limit the size of blood vessels (Bai et al. 2011) and preferably close to 650 to 800 μm in order to have homogeneous bone distribution throughout the scaffold (Abbasi et al. 2020; Mantila Roosa et al. 2010). Pore interconnections shall also be superior to 100 μm to enable good vascularisation of the scaffold, and the larger the interconnection, the larger the blood vessels (Li et al. 2022; Bai et al. 2010).

With the emergence of CAD/CAM technologies, new possibilities have arisen. Subtractive manufacturing, like a 5-axis computer-controlled milling machine, allows producing patient-specific HA blocks (Luongo et al. 2016; Mangano et al. 2022; Mangano et al. 2015). However, this technology does not improve the HA block porosity. On the other hand, ceramic additive manufacturing enables overcoming these HA block limitations by providing to the scaffold a controlled interconnected macroporous structure (Vaquette et al. 2022). Several studies on the optimal macroporosity structure for osseointegration have been conducted with particular attention to the triply periodic minimal surface (TPMS) structures (Maevskaia et al. 2024; Maevskaia et al. 2023). The latter provide an ideal balance between porosity and mechanical strength (Montazerian et al. 2017), have a surface curvature similar to trabecular bone (Charbonnier et al. 2020) and facilitate angiogenesis (Wu et al. 2022). Among the TPMS, gyroids have demonstrated superior results in vertical bone growth compared to particulates and lattice structures (van Hede et al. 2022) and faster mineralization compared to bovine bone blocks (Bouakaz et al. 2023). In addition, the gyroid 3D-printed HA (gyroid-3DHA) has already proven to be effective in clinical use for maxillofacial bone apposition, such as mandibular angle and zygomatic bone augmentations (Systermans et al. 2024; Verbist et al. 2024).

Gyroid-3DHA could also greatly benefit patients with challenging alveolar ridge augmentations: those with severe vertical bone loss, individuals needing both bone reconstruction and implants after trauma or tumour removal, and patients with previous failed bone grafts where conventional methods were inadequate. The ability to customize graft geometry based on patient anatomy and dental implant planning, while maintaining consistent internal architecture, could allow surgeons to address complex three-dimensional defects that are currently difficult to reconstruct.

While the final purpose of alveolar bone augmentation is the placement and osseointegration of a dental implant, all studies on 3D printed calcium-phosphate based materials for alveolar bone augmentation focus only on the osseointegration of the 3D-printed graft (Mohd et al. 2022).

In the present pilot study, we aim to evaluate the complete clinical situation. We designed a pilot study starting from 3DHA grafting up to the osseointegration of the dental implant. We investigated the fixation and osseointegration of the gyroid-3DHA, the placement of a dental implant through the 3DHA, and the dental implant bone-to-implant contact (BIC) within the grafted area. Additionally, since the gyroid-3DHA scaffold holds significant potential for complex bone augmentation, we designed an animal study mimicking a situation where only one surface provides bone contact.

2 | Material and Methods

2.1 | Ethical Considerations

The animal research was in accordance with Directive 2010/63/EU, the current Belgian regulation on lab animal protection, and ARRIVE guidelines. The study protocol was approved by the CER Groupe Ethical Committee under reference PS-2022-CER-002.

2.2 | Animals and Anaesthesia

The study included four female Göttingen minipigs of 2 years old and a weight from 37 to 44 kg. Animals were acclimatized for at least 2 weeks prior to the first surgery. Body weight was monitored at arrival, before surgeries, and then every 2 weeks until euthanasia. Clinical examinations were performed at arrival, before surgeries, and once a week until euthanasia. Special care was paid to the skin and soft tissues around the surgical sites. Animals were fed with a standard diet (pellet food) and water *ad libitum*. During the 3 days following surgery, the animals received a daily intramuscular injection of Meloxicam (0.4 mg/kg).

All surgeries were conducted under general anaesthesia. Intramuscular injection of Buprenorphine (30 μg/kg) was administered 30 min prior to surgery. General anaesthesia was induced by an intramuscular injection of Xylazine (2 mg/kg), Ketamine (2.2 mg/kg), and Zoletil (4.4 mg/kg). After induction, anaesthesia was maintained with 3%–4% isoflurane. To compensate for any liquid loss during surgery and prevent dehydration, a physiological serum perfusion (10 mL/kg) was administered.

2.3 | Study Design

Study design is illustrated in Figure 1. One 3DHA block was placed on each side of the mandibula of all animals, identified by L for left and R for right. First healing period (T1) was either 8 or 12 weeks. Second healing (T2) period was fixed to 12 weeks (Figure 1).

2.4 | Scaffold

All gyroid-3DHA blocks were manufactured by CERHUM SA (Liège, Belgium). They are made of pure hydroxyapatite and have a fully interconnected gyroid porous structure. The manufacturing, including the porosity design, the additive manufacturing process, and the post-treatment, has been previously described (Bouakaz et al. 2023). Each 3DHA block underwent steam sterilization (134°C, 18 min) prior to surgery.

The 3DHA block was designed to fit all minipigs' mandibles. A custom-made design for each minipig could have been created based on scans and with the 3D-printing manufacturing process previously described (Systermans et al. 2024). However, it was not necessary for the present animal model as the minipigs present a flat surface on the mandibular angle. The standardized volume of the 3DHA block was 1200 mm^2, its dimensions are 20 mm × 12 mm × 5 mm, as depicted in Figure 1. Gyroid-3DHA blocks were designed with two holes for osteosynthesis screws. Sufficient space was left in between the screws to be able to place a dental implant without removing the screws.

2.5 | Surgical Procedures

All surgeries were performed in an operating room, ensuring aseptic conditions.

2.5.1 | T0—Bone Graft Placement

Lateral augmentation was performed on both sides of the mandible for each minipig. The lateral and inferior mandibular borders were exposed through a submandibular skin incision. The soft tissue was dissected to expose the lateral surface of the mandible. A flat surface, away from the dental roots, was identified. The cortical bone was perforated using a small round bur under saline solution irrigation. Perforations were not standardized across surgeries. Fixation holes were drilled through the pilot holes already present in the gyroid-3DHA block. (Figure 1) Osteosynthesis screws (Ø 2 mm, length 7 mm) were placed in the planned holes.

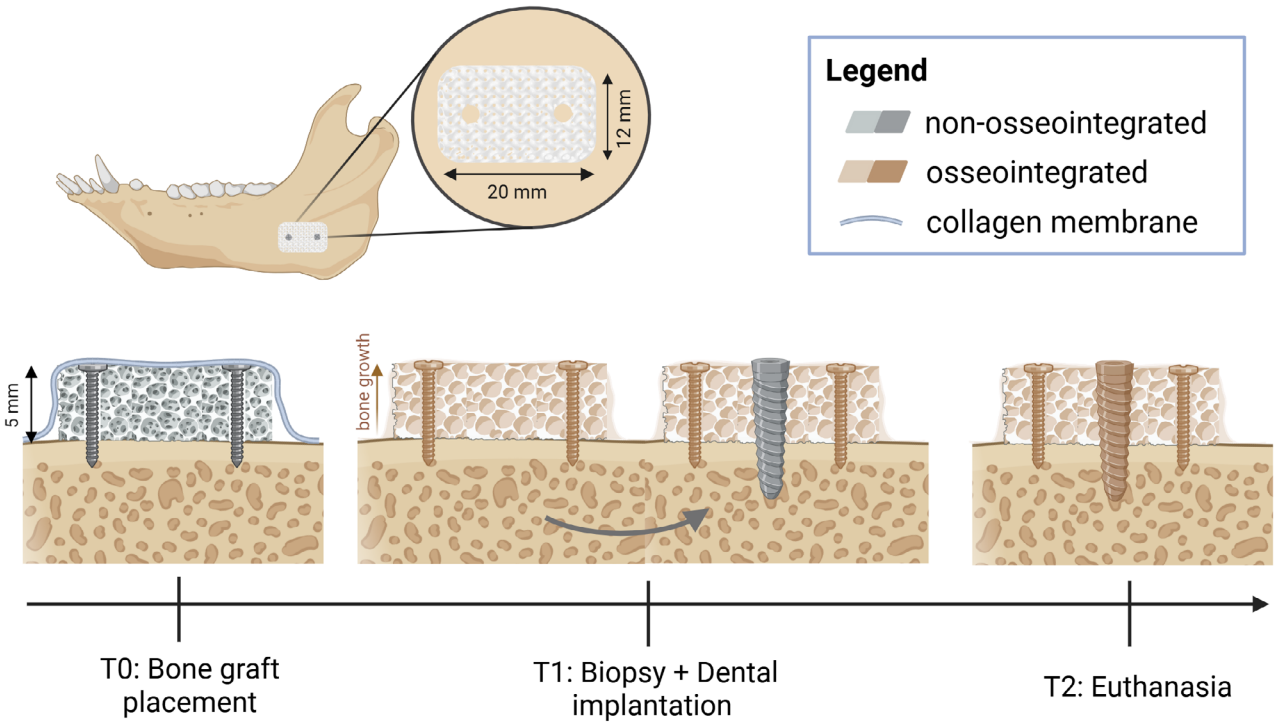

	Specimens	T1	T2
Animal #1	1 L & 1 R	8 weeks	12 weeks
Animal #2	2 L & 2 R	8 weeks	12 weeks
Animal #3	3 L & 3 R	12 weeks	12 weeks
Animal #4	4 L & 4 R	12 weeks	12 weeks

FIGURE 1 | Schematic representation of the animal model including the 3DHA size, bone augmentation location, fixation, and healing periods.

The gyroid-3DHA block was covered with a resorbable collagen membrane (Collprotect, Straumann) fixed with four titanium pins (length 3 mm, Straumann). The surgical site was closed by interrupted sutures in four layers (periosteum, muscle, subcutaneous tissue, and skin) with Vicryl 3–0.

2.5.2 | T1—Dental Implant Placement

A similar incision and dissection were performed to expose the 3DHA block. Implant bed preparation was done in the centre of the 3DHA block first with a needle drill (Ø 1.6 mm, Straumann), then widened with successive pilot drills (Ø 2.2 mm, Ø 2.8 mm, Straumann) and a twist drill (Ø 3.5 mm, Straumann). No implant tapping device was used.

A dental implant (Ø 4.1 mm, RN, SLA 8 mm, Roxolid, Straumann) was inserted with a maximum torque of 35 Ncm as recommended by the manufacturer, and a closure cap was placed.

Additionally, a trephine biopsy of the 3DHA was performed when possible (four specimens out of eight: specimens 1R, 2L, 4L, and 4R). This was done in order to confirm the presence of bone at the time of dental implant placement.

The surgical site was closed by interrupted sutures on four layers (periosteum, muscle, subcutaneous tissue, and skin) with Vicryl 3–0.

2.5.3 | T2—Euthanasia

Euthanasia was performed by pentobarbital injection under general anaesthesia. After the sacrifice of the animals, the mandible was excised, and the left and right hemi-mandibles were separated with a band saw.

2.6 | Histological Preparation

Samples were placed in 4% formaldehyde directly after harvesting. After complete fixation, samples were dehydrated in a graded series of alcohol and embedded in Spurr resin. Screws and dental implants were not removed.

Slide preparation was performed by laser microtomy (TissueSurgeon, LLS ROWIAK LaserLabSolutions), as described by (Kunert-Keil et al. 2019). The obtained slides were undecalcified sections perpendicular to the bone surface in the mesio–distal direction, crossing both screws and the dental implant. Haematoxylin-eosin and McNeal staining were performed.

2.7 | Histopathologic and Histomorphometric Analysis

Histopathologic and histomorphometric analyses were conducted on specimens harvested at T2 with a digital microscope (Olympus BX43). Polarizing light was used to differentiate native lamellar bone and newly formed woven bone. Semiquantitative scoring was performed on inflammation, foreign body reaction, granulocytes, lymphocytes, macrophages, giant cells, fibrosis, new bone formation, remodelling (osteoblasts/osteoclasts), resorption, (osteo-)necrosis, and vascular changes. The scoring scale is: 0 = not present, + = mildly pronounced, ++ = moderately pronounced, +++ = severely pronounced.

Histomorphometric measurements were conducted with CellSens software (Olympus, Hamburg, Germany) and QuPath (Bankhead et al. 2017). The parameters measured are:

- *Total bone gain*: the distance between the native bone surface and the highest new bone location perpendicularly to the native bone surface.
- *Scaffold area*: Augmented surface minus the screws and dental implant areas (Figure 2).
  - New bone area: the surface colonized by new bone within the scaffold area.
  - 3DHA area: surface occupied by the gyroid-3DHA scaffold within the scaffold area.
  - Non-mineralized tissue area: surface occupied by soft tissues, bone marrow, fibrous tissue within the scaffold area.
- *Bone ingrowth*: bone surface percentage within the porosities of the 3DHA.

$$\text{bone ingrowth} = \frac{\text{new bone area}}{\text{scaffold area} - \text{3DHA area}}$$

- *Bone-to-implant contact* (BIC): the percentage of the dental implant surface in direct contact with bone at the microscopic level as the quantitative measurement of its osseointegration. BIC was measured over the full length of the dental implant (Total BIC) and distinguished between the area inside the 3D HA blocks (BIC—3DHA) and the area within the native bone (BIC—Native bone) (Figure 2).

2.8 | Statistical Analysis

As a feasibility pilot study, a formal sample size calculation was not achievable. Instead, four animals (eight surgical sites) were

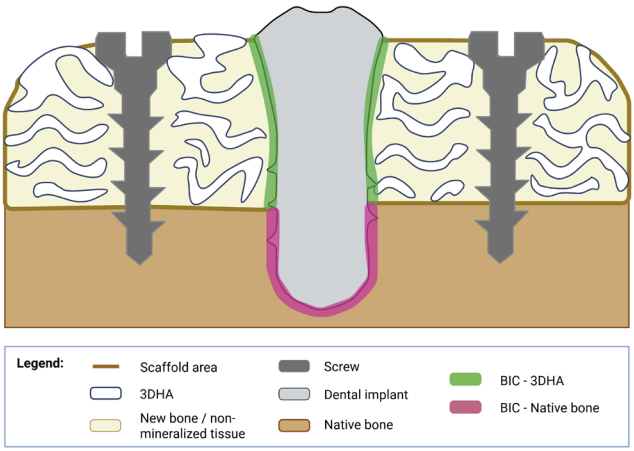

FIGURE 2 | Schematic representations of the regions of interest of the histomorphometric analysis. Transversal section of the scaffold area crossing the dental implant and both screws.

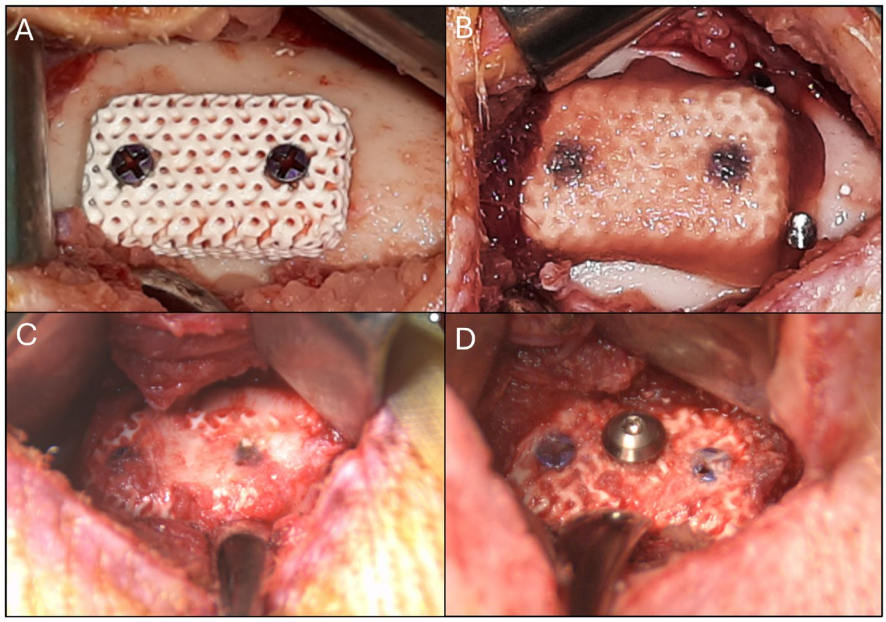

FIGURE 3 | Intra-operative pictures at T0 (A, B) and T1 (C, D). (A) 3DHA fixed with 2 screws. (B) Collagen membrane covering the graft. (C) Osseointegrated 3DHA after the first healing period. New bone is visible macroscopically on the 3DHA surface. (D) Dental implant placed inside the 3DHA.

used, providing adequate preliminary data while adhering to ethical standards.

Descriptive statistics were performed on histomorphometric measurements, including mean +/− standard deviation. Data set normality was verified with the Shapiro–Wilk test. *t*-tests were performed using Prism v10.4.1 (GraphPad) whenever required and possible. For all analyses, differences at $p < 0.05$ were considered statistically significant.

3 | Results

3.1 | Clinical Assessment

Surgeries and postoperative healing were uneventful for all animals for both surgeries. All gyroid-3DHA blocks were successfully placed with 2 screws and a coverage membrane (Figure 3A,B). No breakage of the 3DHA blocks was observed. At T1, new bone was visible through the pores of the graft and sometimes on top of it (Figure 3C). Dental implants were placed at T1 according to standard protocol with good primary retention; 35 Ncm was reached for all (Figure 3D).

One animal (#3) developed a cough and acute dyspnea and died prematurely at T1 + 6 weeks. The absence of any link between the surgery and graft material was confirmed by autopsy.

3.2 | Descriptive Histology and Semi-Quantitative Histopathology

Biopsies were conducted at T1 on four specimens, only for qualitative assessment of bone ingrowth. Biopsies of specimens 2 L, 4 L, and 4 R confirmed the presence of bone inside the 3DHA at the time of dental implantation and already significant bone growth (Figure 4A). Biopsy of specimen 1 R indicated the presence of a severe inflammatory reaction.

Semi-quantitative analysis of the specimens at T2 is presented in Table 1. New bone formation is found inside every gyroid-3DHA specimen. Woven bone is found in direct contact with the 3DHA and in contact with the native lamellar bone (Figure 4B). The direct bone contact between the 3DHA and the new bone, without any fibrous interface, demonstrates the good osseointegration of the bone graft. Notably, the new bone formation and bone remodelling are the highest for animal #4, with the longer follow-up period (T1 + T2), while the fibrosis level is the lowest. Active bone remodelling is highlighted by the presence of multiple cement lines and repeated detections of numerous osteoblasts in all specimens (Figure 4C). Numerous vascular proliferations are evident throughout the entire bone-grafted area (Figure 4D). Bone is found in direct contact with the dental implant within the scaffold area (Figure 4E). In some locations, connective tissues are also found in direct contact with the dental implant (Figure 4F). Active bone formation towards the dental implant is indicated by the presence of numerous osteoblasts (Figure 4F,G).

Adjacent to the soft tissue (at the top of the grafted area), there is an inflammatory reaction attributed to the normal healing of the soft tissues. However, in one specimen (1R), the inflammatory reaction infiltrated the 3DHA. This specimen also presented signs of bone necrosis. This necrosis was caused by the inflammation and originated in the surrounding soft tissue. It took place prior to the dental implant placement, as indicated by the biopsy of specimen 1R.

3.3 | Histomorphometric Analysis

Histomorphometric measurements of all specimens are presented in Table 2, including animal #3 who died prematurely

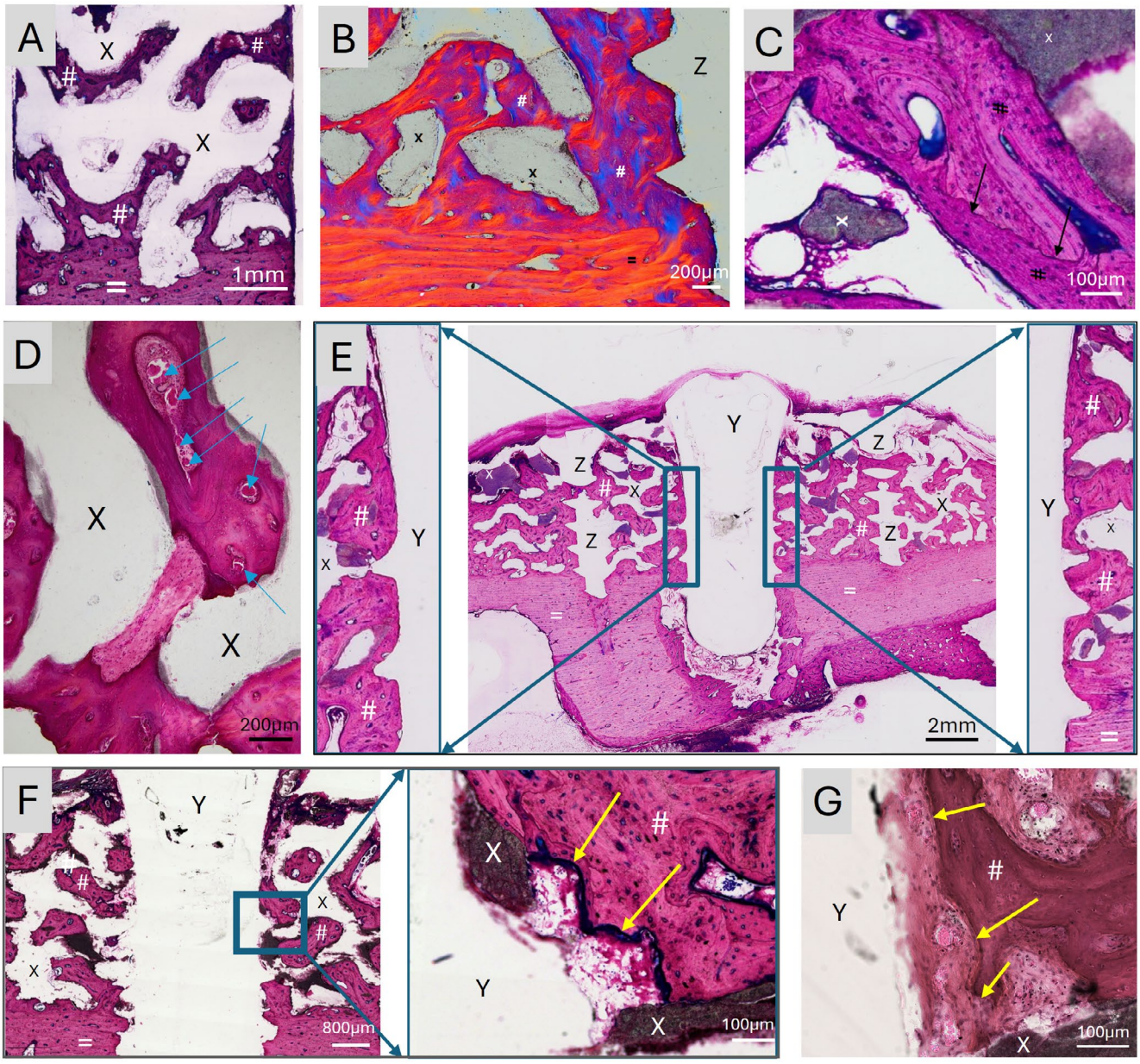

FIGURE 4 | Histological sections. (A) Biopsy sagittal section at T1 (McNeal staining; specimen 4R). (B) Native bone and scaffold area interface (polarized light). (C) Bone remodelling highlighted by cement lines (black arrows) and numerous osteoblasts (McNeal staining). (D) Bloods vessels inside the new bone (blue arrows) (HE staining). (E) Transversal section of the scaffold area highlighting the vertical bone gain, the dental implant placement, and the screws. Interface between dental implant and new bone are enlarged (McNeal staining; specimen 2R). (F) Transversal section of the scaffold area of the dental implant with enlarged view of dental implant—new bone interface (McNeal staining; specimen 3R). (G) Enlarged view of dental implant—new bone interface (HE staining; specimen 3R). Yellow arrows indicate osteoblasts and bone growth towards the dental implant. Legend: 'X': 3DHA; '#': New bone (woven bone); '=': Native cortical bone; 'Y': Dental implant; 'Z': Osteosynthesis screws.

and specimen #1R which presented necrosis. Means are calculated with and without those specimens in Table 2.

3.3.1 | Total Bone Gain

For all except one (1R), the new bone ingrowth reached at least 4 mm of bone augmentation, and in some specimens, it exceeded the 3DHA and peaked at 5.44 mm. Figure 5A illustrates the bone gain across all specimens.

3.3.2 | Bone and Non-Mineralized Tissue Areas

The following data refers to the situation when specimen 1R is excluded (see Table 2 for all specimens' data). The gyroid-3DHA occupies 41.83% of the surface. The new bone covers on average 39.17% of the scaffold area while non-mineralized tissues represent 19%. The bone ingrowth within the 3DHA is on average 67.53%. Bone growth is uninterrupted, starting from the native bone contact surface and uniformly distributed over the cross-section. Non-mineralized tissues are

TABLE 1 | Semiquantitative histopathologic evaluation.

Animal	Side	T1 (weeks)	T2 (weeks)	Inflammation/ foreign body reaction	GranuloctyteS/ lymphocytes	MacrophageS/ giant cells	Fibrosis	New bone formation	RemodeLling (osteoblasts and osteoclasts)	Resorption	(Osteo-) necrosis	Vascular changes	CommentS
1	L	8	12	++_(+++)	++_+++	++_+++	++	++	++	+	_	_	Inflammatory reaction toward the soft tissue and also in the soft tissue with no proximal contact with the bone graft
1	R	8	12	+++	+++	++	+++	+_(++)	(+)_++	+	(++)_+++	_	Inflammatory reaction adjacent to the soft tissue and in the bone graft
2	L	8	12	++_+++	(++)_+++	++	++_(+++)	++	(+)_++	(+)_+	_	_	Inflammatory reaction at the dental implant tip and toward the soft tissue
2	R	8	12	++	++	++	++	++	++	+	_	_	Inflammatory reaction in proximity to soft tissue
3	L	12	6	(+)_++	(+)_++	++	++	++	++	(+)	_	_	Inflammatory reaction in proximity to soft tissue and dental implant neck. Connective tissue adjacent to the dental implant are seen
3	R	12	6	+	+_++	+	++	++	++	(+)	_	_	Connective tissue adjacent to the dental implant are seen
4	L	12	12	+_++	+_++	++	+	+++	++_+++	(+)	_	_	Inflammatory reaction in proximity to soft tissue
4	R	12	12	+_++	+_++	++	(+)	+++	++_+++	(+)	_	_	Inflammatory reaction in proximity to soft tissue and at the dental implant tip, also surrounded by bone marrow

TABLE 2 | Histomorphometric measurements.

				Scaffold area					BIC (%)		
				Mineralized tissues		Non-mineralized tissues (%)	Bone ingrowth (%)	Total bone gain (mm)			
Animals	Side	T1 (weeks)	T2 (weeks)	New bone area (%)	3DHA area (%)				3DHA	Native Bone	Total
1	L	8	12	32.61	39.53	27.89	53.92	4.01	30.42	50.91	42.38
1	R	8	12	3.54	32.71	63.75	5.26	2.51	6.98	5.02	6.10
2	L	8	12	40.68	37.21	22.11	64.79	4.56	20.86	2.49	10.20
2	R	8	12	45.48	35.77	18.75	70.81	4.37	68.45	24.04	46.81
3	L	12	6	38.83	46.81	14.36	73.00	5.00	12.47	17.99	14.98
3	R	12	6	37.40	44.53	18.07	67.42	4.49	14.59	35.79	25.45
4	L	12	12	40.45	45.51	14.04	74.23	5.24	43.04	63.04	54.14
4	R	12	12	38.76	43.47	17.77	68.57	5.44	51.16	30.38	39.16
Mean—all specimens included: (± STD)				**34.72** (±13.10)	**40.69** (±5.13)	**24.59** (±16.43)	**59.75** (±22.90)	**4.45** (±0.92)	**31.00** (±21.53)	**28.71** (±21.08)	**29.90** (±18.17)
Mean—corrected data set: (± STD)				**39.17**[a] (±3.88)	**41.83**[a] (±4.31)	**19.00**[a] (±4.78)	**67.53**[a] (±6.82)	**4.73**[a] (±0.52)	**42.79**[b] (±20.77)	**34.17**[b] (±20.28)	**38.54**[b] (±16.66)

Note: Bold indicates mean values as indicated in the first column.
[a]Specimen 1R is excluded: necrotic graft due to inflammatory reaction.
[b]1R excluded due to necrosis and 3L and 3R excluded due to incomplete T2 healing time.

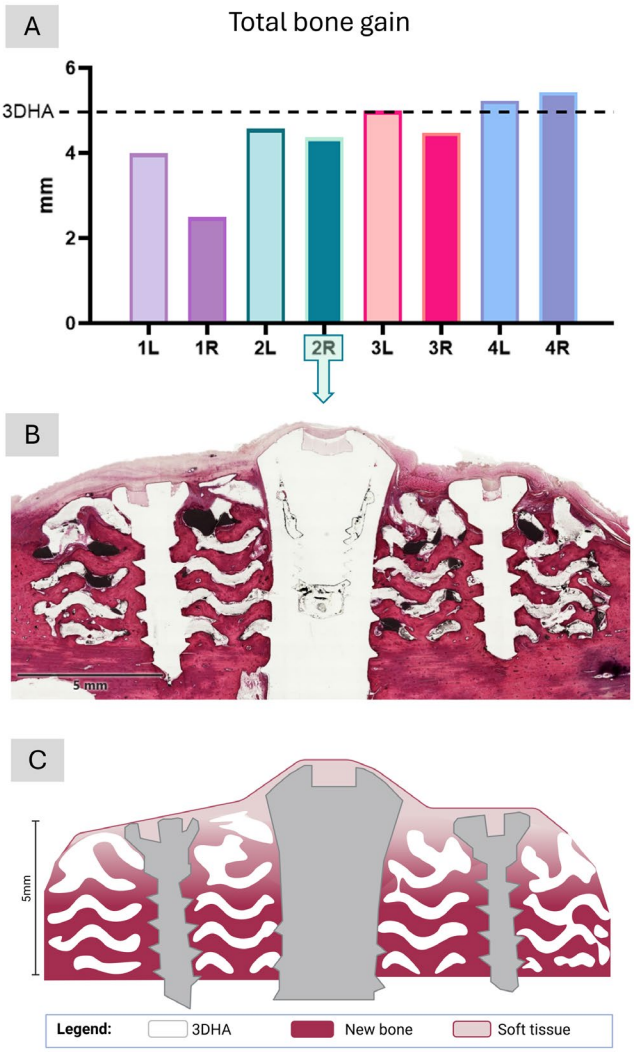

FIGURE 5 | (A) Graphical representation of total bone gain across all specimens. (B) Histological view of specimen #2R (HE staining). (C) Schematic representation of the bone and non-mineralized tissues location throughout the scaffold area with the screws and dental implant (in grey).

mostly constituted of soft tissues located at the top of the bone graft and connective tissue preferably located around the dental implant neck. The tissue distribution is illustrated in Figure 5B,C.

3.3.3 | Bone-To-Implant Contact

BIC percentages in the 3DHA area, in the native and over the full length of the dental implants, are presented in Table 2. Overall, the BIC is slightly higher in the 3DHA (42.79%) compared to the native bone (34.17%), but the difference is not statistically significant.

Regarding the impact of the first healing periods (T1), no noteworthy difference is noticeable between 8 and 12 weeks. However, reduced healing time after dental implant placement (T2), as it is the case for specimens 3L and 3R, led to an incomplete osseointegration of the dental implant (low Total BIC), which is mostly surrounded by connective tissue (Figure 4F).

4 | Discussion

The present pilot study aimed at assessing the 3DHA for its ability to promote lateral bone augmentation in a chronic defect, the possibility of placing a dental implant, and its osseointegration. For the first time, the dental implant osseointegration inside a 3D-printed bone graft has been evaluated.

We demonstrated the feasibility of placing a dental implant inside the 3DHA with the conventional hard bone drilling protocol as in native bone. This ability is important since, in clinical practice, dental implants can be placed across both native bone and bone substitute material. In addition, no fracture of the 3DHA occurred during drilling. Although the fragility of the ceramic scaffold is frequently reported in the literature (Wang and Yeung 2017; James et al. 2020; Piecuch et al. 1990), its mechanical strength improves significantly once the porous structure is filled with new bone (Tamai et al. 2002). This study shows that osseointegrated 3DHA provides sufficient mechanical integrity to withstand drilling and dental implant placement.

In the few previous studies investigating both dental implants and bone substitutes, the placement is either simultaneous (le Thieu et al. 2021; Wen et al. 2017; Catros et al. 2020) or staged (Doi et al. 2016; Mihatovic et al. 2020; Antunes et al. 2013). The present study falls into the second category. Notably, these prior studies often involved a cylindrical-type defect below the critical size (Doi et al. 2016; Mihatovic et al. 2020; Antunes et al. 2013), in an acute phase and supporting spontaneous healing (Mihatovic et al. 2020). The bone substitute's ability to support good and rapid osseointegration is therefore not evaluated.

In contrast, one of the most challenging situations in oral bone augmentation is a chronic defect with minimal native bone contact. This study was designed to replicate such a condition. While cylindrical-type defects have four lateral walls intact, the two-wall defect model removes both lingual and vestibular walls (de Carvalho et al. 2024). In comparison, the model used in the present study represents a chronic defect with only a lateral bone wall (and no others). Although, in our model, there is a possible bias due to the anatomical location allowing periosteal-driven bone formation (Aludden et al. 2020), the situation is still a worst case compared to an acute 1-, 2-, 3-, or 4-wall defect.

The volume of the graft in the present study is two to six times bigger than most other studies. The 3DHA thickness was defined to have a significant part of the dental implant inside the grafted area and be representative of the clinical situation of vertical alveolar bone augmentation. The size of the 3DHA was determined by the space required for placing two screws and one dental implant, which correspond to a usual clinical situation of large bone augmentation. The total volume of the 3DHA block was 1200 mm^3 while others report less than 200 mm^3 in case of a cylindrical-type defect (Mihatovic et al. 2020) and a maximum of up to 500 mm^3 for the biggest appositions (Aludden et al. 2020; Carrel et al. 2016).

The minipig is a frequently used animal model for alveolar bone augmentation and dental implantation studies due to its similarities with human mandibular anatomy and bone remodelling rate (Zhang et al. 2021; Blanc-Sylvestre et al. 2021). However, in contrast to dogs, it is difficult to maintain good oral hygiene with minipigs, and post-operative healing may be jeopardized (Zhang et al. 2021; Blanc-Sylvestre et al. 2021). In the submandibular skin incision model described in the present study and also by others (Aludden et al. 2020; van Oirschot et al. 2022), complications such as wound dehiscence and exposure caused by insufficient oral post-operative care do not arise. However, the anatomical location, being the mandibular bone, remains representative of oral bone augmentation, contrary to the femoral bone chosen by others (Doi et al. 2016) to test dental implants.

In the present study, new bone tissue covered 39.17% of the grafted area. This is largely superior to the porous hydroxyapatite blocks used in the past in maxillofacial surgeries. For the latter, values reported 4.7–16.4 months post-surgery are 48.5% of hydroxyapatite matrix, 18% of new bone, and 33.5% of soft tissue (Cottrell and Wolford 1998). The difference can be explained by the optimized porosity of the gyroid-3DHA blocks. Its fully interconnected and larger pores (Bouakaz et al. 2023) ensure good vascularisation and faster and homogeneous osseointegration.

Bone ingrowth is also satisfying but slightly lower than the 82% previously reported by Aludden et al. (2020) after 20 weeks in a similar anatomical location in a minipig study. However, in Aludden et al.'s study, no dental implant was placed, which is a more favourable situation. Nevertheless, the non-mineralized tissue amounts are within the same range, namely 3%–27% (Aludden et al. 2020). And, similarly to (Wen et al. 2017), inflammation was observed in the soft tissue but not found inside the new bone, for all specimens except 1R.

Although healing periods before dental implant placement vary greatly between minipig studies (from 8 to 32 weeks in post-extraction models), 12 weeks is the most frequent duration (Musskopf et al. 2022). In addition, specifically in the staged implant placement model, the only reported minipig study is based on 12 weeks of healing (Mihatovic et al. 2020). Since previous studies (van Hede et al. 2022; Bouakaz et al. 2023) demonstrated rapid and superior osseointegration properties of gyroid-3DHA bone grafts, investigating a shorter healing period of 8 weeks was of particular interest. In the present study, no difference in BIC was observed between healing periods of 8 and 12 weeks, suggesting that a reduced healing duration before dental implant placement could be feasible when using the gyroid-3DHA block. However, due to the significant variability observed in BIC measurements, further studies with larger sample sizes are necessary to confirm this finding.

Compared to other studies involving a graft material, BIC measurements reported in the present study are similar, highlighting a good osseointegration of the dental implant inside the 3DHA bone graft. For instance, Doi et al. reported a BIC of 34.7% after 12 weeks in dog femurs (Doi et al. 2016), whereas Wen et al. found a BIC of 33.3% after 9 weeks in the mandibular bone of minipigs in their control group without BMP-2 (Wen et al. 2017). Conversely, Mihatovic et al. reported higher BIC values ranging from 73.38% to 84.11% after an 8-week healing period; however, their study involved non-critical size, four-wall bone defects, and notably, the bone substitute material had significantly resorbed (remaining material ranged from 9.2% to 14.04%) (Mihatovic et al. 2020).

Unfortunately, the comparison cannot be brought further due to the differences in animal models, size of graft, and type of defects. Therefore, in order to have an objective assessment of the 3DHA performance, we decided to compare the dental implant BIC in the native bone (dental implant tip) and inside the 3DHA. We have demonstrated a similar BIC in the 3DHA compared to the native bone area. This confirms that the gyroid-3DHA can successfully support dental implants' osseointegration.

As expected, specimen 1R, presenting severe inflammation and osteonecrosis, is also associated with a low BIC. But surprisingly, although specimen 2 L presents a high graft osseointegration (40.68% of new bone), the dental implant is surrounded by connective tissue in large areas, and the BIC is low, especially at the tip inside the native bone. Notably, the dental implant tip is also surrounded by a pronounced mononuclear inflammatory reaction (Table 1).

Of note, one dental implant failed to osseointegrate inside the 3DHA (1R) due to bone graft necrosis caused by inflammation. The exact cause of the inflammation is unknown but could be explained by excessive pressure on the minipig cheek area (Aludden et al. 2020). Surprisingly, another dental implant presented a low BIC inside a well-integrated bone graft (specimen 2 L, new bone area: 40.68%, BIC: 20.86%) and even a lower BIC in the native bone (2.49%). This suggests poor osseointegration unrelated to the graft material. The dental implant is surrounded by connective tissue in large areas, and the dental implant tip is also surrounded by a pronounced mononuclear inflammatory reaction, potentially due to contact with the mandibular canal. Other factors, like thermal osteonecrosis during drilling or micromovements, may have disrupted the healing phase, hindering dental implant osseointegration.

Dental implants with reduced T2 healing time, such as specimens 3L and 3R with 6 weeks instead of 12 weeks, have a lower BIC compared to the other specimens. Notably, connective tissue is found around the dental implant without any inflammatory reaction. It is therefore assumed that this corresponds to immature bone formation and full osseointegration would have been achieved with a complete healing time. In fact, active bone formation by way of numerous osteoblasts is visible next to the dental implant and connective tissue (Figure 4G).

Overall, the animal model used in the present study was more ambitious than previous studies by combining a chronic defect with only a lateral bone wall, a significantly bigger bone graft, and shorter healing periods. But this pilot study presents some limitations as well. The small sample size ($n = 4$), including the premature loss of one animal, reduces statistical power and limits its conclusions about healing duration. The anatomical site used, while convenient, does not fully replicate the oral environment. The absence of a control group prevents direct comparison with standard graft materials. Employing tissue-level implants rather than bone-level implants likely led to underestimated bone-to-implant contact. In fact, the tissue-level implant neck is smooth

to prevent bone tissue attachments, and part of this neck was inside the 3DHA grafts. Finally, the use of standardized grafts does not showcase the full potential of personalized 3D-printed designs.

Patient-specific bone grafts in alveolar bone augmentation bring several advantages such as good bone contacts, precise augmentation according to dental implantation planning, and faster surgeries (Mangano et al. 2022). The clinical use must also consider current higher manufacturing costs of these patient-specific solutions. But these may be offset by potential benefits like reduced operating time, fewer complications, and faster healing. Manufacturing costs are also expected to decrease as the technology matures and production scales up.

Currently, only a few clinical case series of patient-specific grafts in the form of 3D-milled HA blocks (Luongo et al. 2016; Mangano et al. 2022) or allografts (Kloss et al. 2023) have been reported for alveolar ridge augmentation. Regarding 3D-printed ceramic grafts, a few recent case reports have been published (Johansson et al. 2024; Perez et al. 2023; Schönegg et al. 2024). However, these cases are currently limited to horizontal bone augmentation and do not capture the full potential of 3D-printed bone grafts.

To investigate further the gyroid-3DHA, a comparative study with an intra-oral defect previously healed and implying a vertical augmentation could be set up. CT scan prior to bone augmentation surgery should be performed to enable customized design of the bone graft. It is important to examine closer patient-specific gyroid-3DHA blocks to better highlight its critical advantages in alveolar bone augmentation. Ultimately fixation of the 3DHA directly with the dental implant could be investigated also.

Overall, this study's outcomes reveal valuable potential for clinical practice, particularly benefiting patients who require extensive alveolar ridge reconstruction prior to implant placement. The combination of customizable graft geometries with predictable implant integration could significantly enhance outcomes for challenging cases lacking effective treatment alternatives. Although larger-scale comparative studies are required to further substantiate these preliminary findings, this pilot study lays the groundwork for innovative alveolar ridge augmentation. Integrating digital planning, 3D-printing technology, and conventional implant techniques represents a promising advancement in reconstructive dental surgery.

5 | Conclusion

In conclusion, to the best of our knowledge, it is the first time a 3D-printed bone substitute is studied together with a dental implant in an animal study. The present pilot study confirms the great potential of gyroid-3DHA for alveolar bone augmentation. Compatibility with standard dental implant protocols is confirmed and clinically relevant. Comparable bone-to-implant contact was observed between dental implant in 3DHA and native bone (42.79% vs. 34.17%). Results achieved after only 8 weeks of healing suggest potential for faster clinical protocols. However, further investigation is needed to overcome the limitations of this pilot study, mainly the small sample size and the absence of a control group.

Author Contributions

Simon Systermans: conceptualization, methodology, investigation, data curation, validation, formal analysis, writing – original draft, writing – review and editing. **Christophe Ronsmans:** conceptualization, investigation, writing – review and editing. **Grégory Nolens:** conceptualization, supervision, funding acquisition, writing – review and editing. **Joeri Meyns:** methodology, writing – review and editing, validation. **Yves Gilon:** supervision, writing – review and editing, methodology. **Elisabeth Cobraiville:** conceptualization, methodology, data curation, validation, formal analysis, visualization, writing – original draft, writing – review and editing.

Acknowledgements

The authors would like to thank Sarah De Lievre for her help with illustrations and data analysis and Dr. Benita Hermanns-Sachweh for histopathology and histomorphometry analysis Figures 1, 2 and 5C were created in Biorender, accessible respectively to the following links: https://BioRender.com/3pdgm06; https://BioRender.com/d4lca8f; https://BioRender.com/azchgjx.

Ethics Statement

The animal research was in accordance with the Directive 2010/63/EU, the current Belgian regulation on lab animal protection, and ARRIVE guidelines. The study protocol was approved by the CERGroupe Ethical Committee under reference PS-2022-CER-002.

Conflicts of Interest

E.C. is a CERHUM employee. G.N. has direct ownership in CERHUM and its patents. The other authors have no conflicts of interest. The co-authors E.C. and G.N. mention that the compound 3DHA evaluated is commercially available from the Cerhum company, Belgium. This did not alter in any way the scientific data provided, which were acquired independently.

Data Availability Statement

The data that support the findings of this study are available from the corresponding author upon reasonable request.

References

Abbasi, N., S. Hamlet, R. M. Love, and N. T. Nguyen. 2020. "Porous Scaffolds for Bone Regeneration." *Journal of Science: Advanced Materials and Devices* 5: 1–9. https://doi.org/10.1016/J.JSAMD.2020.01.007.

Aludden, H., A. Mordenfeld, C. Dahlin, M. Hallman, and T. Starch-Jensen. 2020. "Histological and Histomorphometrical Outcome After Lateral Guided Bone Regeneration Augmentation of the Mandible With Different Ratios of Deproteinized Bovine Bone Mineral and Autogenous Bone. A Preclinical In Vivo Study." *Clinical Oral Implants Research* 31: 1025–1036. https://doi.org/10.1111/clr.13649.

Alyahya, A., and G. R. J. Swennen. 2019. "Bone Grafting in Orthognathic Surgery: A Systematic Review." *International Journal of Oral and Maxillofacial Surgery* 48: 322–331. https://doi.org/10.1016/J.IJOM.2018.08.014.

Antunes, A. A., P. Oliveira Neto, E. de Santis, M. Caneva, D. Botticelli, and L. A. Salata. 2013. "Comparisons Between Bio-Oss and Straumann Bone Ceramic in Immediate and Staged Implant Placement in Dogs

Mandible Bone Defects." *Clinical Oral Implants Research* 24: 135–142. https://doi.org/10.1111/j.1600-0501.2011.02385.x.

Bai, F., Z. Wang, J. Lu, et al. 2010. "The Correlation Between the Internal Structure and Vascularization of Controllable Porous Bioceramic Materials In Vivo: A Quantitative Study." *Tissue Engineering, Part A* 16: 3791–3803. https://doi.org/10.1089/TEN.TEA.2010.0148/FORMAT/EPUB.

Bai, F., J. Zhang, Z. Wang, et al. 2011. "The Effect of Pore Size on Tissue Ingrowth and Neovascularization in Porous Bioceramics of Controlled Architecture In Vivo." *Biomedical Materials* 6: 15007. https://doi.org/10.1088/1748-6041/6/1/015007.

Bankhead, P., M. B. Loughrey, J. A. Fernández, et al. 2017. "QuPath: Open Source Software for Digital Pathology Image Analysis." *Scientific Reports* 7: 1–7. https://doi.org/10.1038/s41598-017-17204-5.

Blanc-Sylvestre, N., P. Bouchard, C. Chaussain, and C. Bardet. 2021. "Pre-Clinical Models in Implant Dentistry: Past, Present, Future." *Biomedicine* 9: 1538. https://doi.org/10.3390/biomedicines9111538.

Bouakaz, I., C. Drouet, D. Grossin, E. Cobraiville, and G. Nolens. 2023. "Hydroxyapatite 3D-Printed Scaffolds With Gyroid-Triply Periodic Minimal Surface Porous Structure: Fabrication and an In Vivo Pilot Study in Sheep." *Acta Biomaterialia* 170: 580–595. https://doi.org/10.1016/j.actbio.2023.08.041.

Carrel, J. P., A. Wiskott, S. Scherrer, and S. Durual. 2016. "Large Bone Vertical Augmentation Using a Three-Dimensional Printed TCP/HA Bone Graft: A Pilot Study in Dog Mandible." *Clinical Implant Dentistry and Related Research* 18: 1183–1192. https://doi.org/10.1111/cid.12394.

Catros, S., R. Sandgren, B. Pippenger, J. Fricain, V. Herber, and E. El Chaar. 2020. "A Novel Xenograft Bone Substitute Supports Stable Bone Formation in Circumferential Defects Around Dental Implants in Minipigs." *International Journal of Oral & Maxillofacial Implants* 35: 1122–1131. https://doi.org/10.11607/JOMI.8265.

Chao, Y.-C., P.-C. Chang, J.-H. Fu, H.-L. Wang, and H.-L. Chan. 2017. "Surgical Site Assessment for Soft Tissue Management in Ridge Augmentation Procedures." *International Journal of Periodontics & Restorative Dentistry* 35: e75–e83. https://doi.org/10.11607/prd.2097.

Charbonnier, B., M. Manassero, M. Bourguignon, et al. 2020. "Custom-Made Macroporous Bioceramic Implants Based on Triply-Periodic Minimal Surfaces for Bone Defects in Load-Bearing Sites." *Acta Biomaterialia* 109: 254–266. https://doi.org/10.1016/J.ACTBIO.2020.03.016.

Cottrell, D. A., and L. M. Wolford. 1998. "Long-Term Evaluation of the Use of Coralline Hydroxyapatite in Orthognathic Surgery." *Journal of Oral and Maxillofacial Surgery* 56: 935–941. https://doi.org/10.1016/S0278-2391(98)90654-1.

de Carvalho, B., E. Dory, C. Trus, et al. 2024. "Biological Performance of a Novel Bovine Hydroxyapatite in a Guided Bone Regeneration Model: A Preclinical Study in a Mandibular Defect in Dogs." *Clinical Implant Dentistry and Related Research* 26: 183–196. https://doi.org/10.1111/CID.13260.

Doi, K., T. Kubo, Y. Makihara, et al. 2016. "Osseointegration Aspects of Placed Implant in Bone Reconstruction With Newly Developed Block-Type Interconnected Porous Calcium Hydroxyapatite." *Journal of Applied Oral Science* 24: 325–331. https://doi.org/10.1590/1678-775720150597.

Ferraz, M. P. 2023. "Bone Grafts in Dental Medicine: An Overview of Autografts, Allografts and Synthetic Materials." *Materials* 16: 4117. https://doi.org/10.3390/ma16114117.

Habraken, W., P. Habibovic, M. Epple, and M. Bohner. 2016. "Calcium Phosphates in Biomedical Applications: Materials for the Future?" *Materials Today* 19: 69–87. https://doi.org/10.1016/j.mattod.2015.10.008.

Hou, X., L. Zhang, Z. Zhou, et al. 2022. "Calcium Phosphate-Based Biomaterials for Bone Repair." *Journal of Functional Biomaterials* 13: 187. https://doi.org/10.3390/jfb13040187.

Hupp, J. R., and S. J. McKenna. 1988. "Use of Porous Hydroxylapatite Blocks for Augmentation of Atrophic Mandibles." *Journal of Oral and Maxillofacial Surgery* 46: 538–545. https://doi.org/10.1016/0278-2391(88)90143-7.

James, C., D. Kathryn, and C. Martin. 2020. "Use of Xenograft Bone Block for Staged Ridge Augmentation Prior to Dental Implant Placement in Trauma Patients." *Faculty Dental Journal* 11: 96–101. https://doi.org/10.1308/Rcsfdj.2020.93.

Johansson, L., J. L. Latorre, M. Liversain, E. Thorel, Y. Raymond, and M. P. Ginebra. 2024. "Three-Dimensional Printed Patient-Specific Vestibular Augmentation: A Case Report." *Journal of Clinical Medicine* 13: 2408. https://doi.org/10.3390/jcm13082408.

Kattimani, V. S., S. Kondaka, and K. P. Lingamaneni. 2016. "Hydroxyapatite-Past, Present, and Future in Bone Regeneration, Bone Tissue Regen Insights." *Bone and Tissue* 7: BTRI.S36138. https://doi.org/10.4137/btri.s36138.

Kloss, F. R., P. W. Kämmerer, and A. Kloss-Brandstätter. 2023. "Risk Factors for Complications Following Staged Alveolar Ridge Augmentation and Dental Implantation: A Retrospective Evaluation of 151 Cases With Allogeneic and 70 Cases With Autogenous Bone Blocks." *Journal of Clinical Medicine* 12: 6. https://doi.org/10.3390/jcm12010006.

Kunert-Keil, C., H. Richter, I. Zeidler-Rentzsch, I. Bleeker, and T. Gredes. 2019. "Histological Comparison Between Laser Microtome Sections and Ground Specimens of Implant-Containing Tissues." *Annals of Anatomy* 222: 153–157. https://doi.org/10.1016/j.aanat.2018.12.001.

le Thieu, M. K., A. Homayouni, L. R. Hæren, et al. 2021. "Impact of Simultaneous Placement of Implant and Block Bone Graft Substitute: An In Vivo Peri-Implant Defect Model." *Biomaterials Research* 25: 43. https://doi.org/10.1186/s40824-021-00245-3.

Li, J., H. Huang, T. Xu, et al. 2022. "Effect of the Interconnecting Window Diameter of Hydroxyapatite Scaffolds on Vascularization and Osteoinduction." *Ceramics International* 48: 25070–25078. https://doi.org/10.1016/J.CERAMINT.2022.05.162.

Luongo, F., F. G. Mangano, A. Macchi, G. Luongo, and C. Mangano. 2016. "Custom-Made Synthetic Scaffolds for Bone Reconstruction: A Retrospective, Multicenter Clinical Study on 15 Patients." *BioMed Research International* 2016: 1–12. https://doi.org/10.1155/2016/5862586.

Maevskaia, E., C. Ghayor, I. Bhattacharya, J. Guerrero, and F. E. Weber. 2024. "TPMS Microarchitectures for Vertical Bone Augmentation and Osteoconduction: An In Vivo Study." *Materials* 17: 2533. https://doi.org/10.3390/ma17112533.

Maevskaia, E., J. Guerrero, C. Ghayor, I. Bhattacharya, and F. E. Weber. 2023. "Triply Periodic Minimal Surface-Based Scaffolds for Bone Tissue Engineering: A Mechanical, In Vitro and In Vivo Study." *Tissue Engineering, Part A* 29: 507–517. https://doi.org/10.1089/ten.tea.2023.0033.

Mangano, C., G. Luongo, F. Luongo, et al. 2022. "Custom-Made Computer-Aided-Design/Computer-Assisted-Manufacturing (CAD/CAM) Synthetic Bone Grafts for Alveolar Ridge Augmentation: A Retrospective Clinical Study With 3 Years of Follow-Up." *Journal of Dentistry* 127: 104323. https://doi.org/10.1016/j.jdent.2022.104323.

Mangano, F. G., P. A. Zecca, R. Van Noort, et al. 2015. "Custom-Made Computer-Aided-Design/Computer-Aided-Manufacturing Biphasic Calcium-Phosphate Scaffold for Augmentation of an Atrophic Mandibular Anterior Ridge." *Case Reports in Dentistry* 2015: 941265. https://doi.org/10.1155/2015/941265.

Mantila Roosa, S. M., J. M. Kemppainen, E. N. Moffitt, P. H. Krebsbach, and S. J. Hollister. 2010. "The Pore Size of Polycaprolactone Scaffolds

Has Limited Influence on Bone Regeneration in an In Vivo Model." *Journal of Biomedical Materials Research. Part A* 92: 359–368. https://doi.org/10.1002/JBM.A.32381.

Mihatovic, I., F. Schwarz, K. Obreja, et al. 2020. "Staged Implant Placement After Defect Regeneration Using Biphasic Calcium Phosphate Materials With Different Surface Topographies in a Minipig Model." *Clinical Oral Investigations* 24: 3289–3298. https://doi.org/10.1007/S00784-020-03206-7.

Mohd, N., M. Razali, M. J. Ghazali, and N. H. A. Kasim. 2022. "3D-Printed Hydroxyapatite and Tricalcium Phosphates-Based Scaffolds for Alveolar Bone Regeneration in Animal Models: A Scoping Review." *Materials* 15: 2621. https://doi.org/10.3390/ma15072621.

Montazerian, H., E. Davoodi, M. Asadi-Eydivand, J. Kadkhodapour, and M. Solati-Hashjin. 2017. "Porous Scaffold Internal Architecture Design Based on Minimal Surfaces: A Compromise Between Permeability and Elastic Properties." *Materials and Design* 126: 98–114. https://doi.org/10.1016/j.matdes.2017.04.009.

Musskopf, M. L., A. F. Stadler, U. M. E. Wikesjö, and C. Susin. 2022. "The Minipig Intraoral Dental Implant Model: A Systematic Review and Meta-Analysis." *PLoS One* 17: e0264475. https://doi.org/10.1371/journal.pone.0264475.

Perez, A., B. Lazzarotto, L. Marger, and S. Durual. 2023. "Alveolar Ridge Augmentation With 3D -Printed Synthetic Bone Blocks: A Clinical Case Series." *Clinical Case Reports* 11: e7171. https://doi.org/10.1002/ccr3.7171.

Piecuch, J. F., A. Ponichtera, and H. Nikoukari. 1990. "Long-Term Evaluation of Porous Hydroxyapatite Blocks for Alveolar Ridge Augmentation." *International Journal of Oral and Maxillofacial Surgery* 19: 147–150. https://doi.org/10.1016/S0901-5027(05)80131-6.

Sanz-Sánchez, I., I. Sanz-Martín, A. Ortiz-Vigón, A. Molina, and M. Sanz. 2022. "Complications in Bone-Grafting Procedures: Classification and Management." *Periodontology 2000* 2000, no. 88: 86–102. https://doi.org/10.1111/PRD.12413.

Schönegg, D., H. Essig, A. Al-Haj Husain, F. E. Weber, and S. Valdec. 2024. "Patient-Specific Beta-Tricalcium Phosphate Scaffold for Customized Alveolar Ridge Augmentation: A Case Report." *International Journal of Implant Dentistry* 10: 21. https://doi.org/10.1186/s40729-024-00541-2.

Systermans, S., E. Cobraiville, S. Camby, et al. 2024. "An Innovative 3D Hydroxyapatite Patient-Specific Implant for Maxillofacial Bone Reconstruction: A Case Series of 13 Patients." *Journal of Cranio-Maxillofacial Surgery* 52: 420–431. https://doi.org/10.1016/j.jcms.2024.02.026.

Tamai, N., A. Myoui, T. Tomita, et al. 2002. "Novel Hydroxyapatite Ceramics With an Interconnective Porous Structure Exhibit Superior Osteoconduction In Vivo." *Journal of Biomedical Materials Research* 59: 110–117. https://doi.org/10.1002/JBM.1222.

Urban, I. A., E. Montero, E. Amerio, D. Palombo, and A. Monje. 2023. "Techniques on Vertical Ridge Augmentation: Indications and Effectiveness." *Periodontology 2000* 93: 153–182. https://doi.org/10.1111/prd.12471.

van Hede, D., B. Liang, S. Anania, et al. 2022. "3D-Printed Synthetic Hydroxyapatite Scaffold With In Silico Optimized Macrostructure Enhances Bone Formation In Vivo." *Advanced Functional Materials* 32: 2105002. https://doi.org/10.1002/adfm.202105002.

van Oirschot, B. A. J. A., E. J. W. Geven, A. G. Mikos, J. J. J. P. van den Beucken, and J. A. Jansen. 2022. "A Mini-Pig Mandibular Defect Model for Evaluation of Craniomaxillofacial Bone Regeneration." *Tissue Engineering. Part C, Methods* 28: 193–201. https://doi.org/10.1089/ten.tec.2022.0012.

Vaquette, C., J. Mitchell, and S. Ivanovski. 2022. "Recent Advances in Vertical Alveolar Bone Augmentation Using Additive Manufacturing Technologies." *Frontiers in Bioengineering and Biotechnology* 9: 798393. https://doi.org/10.3389/FBIOE.2021.798393/BIBTEX.

Verbist, M., A.-L. Vandevelde, J. Geusens, Y. Sun, E. Shaheen, and R. Willaert. 2024. "Reconstruction of Craniomaxillofacial Bone Defects With 3D-Printed Bioceramic Implants: Scoping Review and Clinical Case Series." *Journal of Clinical Medicine* 13: 2805. https://doi.org/10.3390/jcm13102805.

Wang, W., and K. W. K. Yeung. 2017. "Bone Grafts and Biomaterials Substitutes for Bone Defect Repair: A Review." *Bioactive Materials* 2: 224–247. https://doi.org/10.1016/j.bioactmat.2017.05.007.

Wen, B., D. Shafer, P. Schleier, D. Pendrys, L. Kuhn, and M. Freilich. 2017. "Implant-Guided Supracrestal Alveolar Bone Growth Using Scaffolds, BMP-2, and Novel Scaffold-Retaining Device." *Clinical Oral Implants Research* 28: 1411–1420. https://doi.org/10.1111/clr.13005.

White, E., and E. C. Shors. 1986. "Biomaterial Aspects of Interpore-200 Porous Hydroxyapatite." *Dental Clinics of North America* 30: 49–67. https://doi.org/10.1016/s0011-8532(22)02094-8.

Wu, F., J. Yang, X. Ke, et al. 2022. "Integrating Pore Architectures to Evaluate Vascularization Efficacy in Silicate-Based Bioceramic Scaffolds." *Regenerative Biomaterials* 9: rbab077. https://doi.org/10.1093/rb/rbab077.

Yoshikawa, H., N. Tamai, T. Murase, and A. Myoui. 2008. "Interconnected Porous Hydroxyapatite Ceramics for Bone Tissue Engineering." *Journal of the Royal Society, Interface* 6: S341. https://doi.org/10.1098/RSIF.2008.0425.FOCUS.

Zecha, P. J., J. Schortinghuis, J. E. van der Wal, et al. 2011. "Applicability of Equine Hydroxyapatite Collagen (eHAC) Bone Blocks for Lateral Augmentation of the Alveolar Crest. A Histological and Histomorphometric Analysis in Rats." *International Journal of Oral and Maxillofacial Surgery* 40: 533–542. https://doi.org/10.1016/J.IJOM.2011.01.007.

Zhang, Z., Y. Gan, Y. Guo, X. Lu, and X. Li. 2021. "Animal Models of Vertical Bone Augmentation (Review)." *Experimental and Therapeutic Medicine* 22: 919. https://doi.org/10.3892/etm.2021.10351.